

---

# Learning to Defer under Expert Drift

---

Anonymous Author  
Anonymous Institution

## Abstract

The *learning to defer* (L2D) framework enables safety in machine learning and AI systems by allocating difficult or critical decisions to a human expert. However, prior work on L2D assumes fixed expert reliability, overlooking temporal fluctuations in human performance due to factors such as fatigue and cognitive biases. Humans commonly exhibit such substantial, systematic performance shifts in high-stakes domains such as radiology, aviation, and driving. We propose *Expert Drift Adapted Learning-to-Defer* (EDA-L2D), a novel expert-aware L2D framework that explicitly models these temporal shifts by conditioning the deferral head on recent histories of expert outcomes via a sequence model. This history-aware approach enables adaptive deferral policies that anticipate reliability fluctuations and better allocate decisions between human and machine over time. We provide comprehensive experiments across 3 diverse tasks - image classification, medical diagnosis, and hate speech detection - showing that for a time-dependent expert, our approach consistently achieves higher performance and better deferral rates than prior L2D approaches.

## 1 INTRODUCTION

*Hybrid intelligent* (HI) systems combine human and machine intelligence to achieve goals unattainable by either alone, emphasizing complementarity over replacement (Kamar, 2016; Dellermann et al., 2019; Akata et al., 2020). One popular HI paradigm is *learning to defer* (L2D): the system learns not only to predict a label but also to decide when to hand off the decision

to a human expert. The original formulation of L2D shows that accounting for the expert’s strengths and biases can improve overall accuracy and fairness relative to a static rejection framework (Madras et al., 2018).

However, existing L2D systems assume that expert behavior is fixed or stationary. In practice, human performance often varies significantly over time due to fatigue (Figalová et al., 2024; Peukert et al., 2023; Pan et al., 2022; Bruni et al., 2012) and various cognitive biases (Legler et al., 2025; Urai et al., 2019; van de Wouw et al., 2024). We show real-world evidence of this effect on a widely studied computer vision task, CIFAR10, by analyzing real human label data from over 2,500 human annotators in the CIFAR10H dataset (Joshua et al., 2019). We show in Fig. 1 that there exists a slight but consistent decline in annotator accuracy over time: the more examples the annotators label, the less accurate they are at producing correct labels. This is a notable observation: CIFAR10 is a relatively simple task (image classification over only 10 classes of common objects), yet even on such a simple task, we observe annotator fatigue. This motivates developing a L2D approach that can account for these structured temporal shifts, in turn allowing it to naturally model and adapt to real human experts.

We address this challenge by proposing a novel framework for L2D: *Expert-Drift-Adapted Learning to Defer* (EDA-L2D). Our framework explicitly models non-stationarity in expert performance. We modify L2D’s rejector sub-component to condition on short-horizon histories of expert decisions. This allows the system to be aware of the expert’s current behavior, and modify its deferral policy accordingly. We illustrate our approach Fig. 2a. Concretely, we integrate a sequence model into the deferral head to explicitly model expert reliability over time. We validate our approach across diverse tasks including medical image recognition, hate speech detection, and image classification. We demonstrate consistent gains in system accuracy over existing, time-agnostic L2D approaches. In summary, our contributions are as follows:

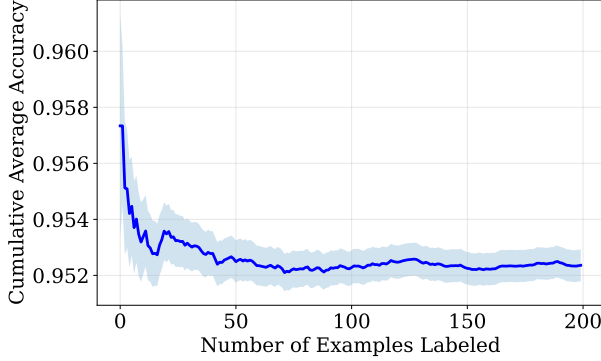


Figure 1: *Annotator Fatigue in CIFAR-10-H.* After removing attention checks, we compute the average cumulative accuracy across all 2,555 human annotators at each time-step. We observe a slight but clear downward drift in performance over time.

- We propose a novel *Expert-Drift-Adapted Learning to Defer* (EDA-L2D) that explicitly models variance in human expert performance over time, allowing the system to flexibly adapt to realistic human experts. We propose our approach in §3, including a new time-aware learning objective (§3.2) and model formulation (§3.3).
- We validate the approach with simulated, time-dependent experts on real-world tasks that require HI solutions (§4.1, §4.2, §4.3), and show that this time-variance is present in real human-annotated data (Fig.1).

## 2 BACKGROUND

We first describe the traditional L2D setting (Mozannar and Sontag, 2021), in which the expert’s abilities are assumed to be static and time-invariant.

### 2.1 Data & Models

We will exclusively consider the problem of multi-class classification with a feature space  $\mathcal{X}$  and the label space  $\mathcal{Y} = \{1, \dots, K\}$ . Given some input  $x \in \mathcal{X}$ , we define  $\mathbb{P}(y | x)$  as the unknown label-generating distribution and  $\mathbb{P}(m | x)$  as the unknown distribution over expert predictions  $m \in \mathcal{Y}$ . L2D is comprised of two sub-components: a *classifier*  $h : \mathcal{X} \rightarrow \mathcal{Y}$  and a *rejector*  $r : \mathcal{X} \rightarrow \{0, 1\}$ , which decides whether to make a prediction using the classifier ( $r(x) = 0$ ) or by deferring to the expert ( $r(x) = 1$ ).

### 2.2 Classifier-Rejector Loss Function

To train our L2D model, we need to fit both the rejector and classifier models. The classifier incurs a loss of zero

(correct) or one (incorrect) when it makes a prediction. Similarly, the human expert incurs the same 0-1 loss when making a prediction (i.e.  $r(\mathbf{x}) = 1$ ). Combining these two 0-1 losses using the rejector model results in the combined classifier-rejector loss:

$$L_{0-1}(h, r) = \mathbb{E}_{\mathbf{x}, y, m} [(1 - r(\mathbf{x})) \mathbb{I}[h(\mathbf{x}) \neq y] + r(\mathbf{x}) \mathbb{I}[m \neq y]] \quad (1)$$

where  $\mathbb{I}$  denotes an indicator function checking the prediction against the ground-truth label. When minimizing this loss, the resulting Bayes optimal classifier and rejector satisfy:

$$\begin{aligned} h^*(\mathbf{x}) &= \arg \max_{y \in \mathcal{Y}} \mathbb{P}(y = y | \mathbf{x}), \\ r^*(\mathbf{x}) &= \mathbb{I} \left[ \mathbb{P}(m = y | \mathbf{x}) \geq \max_{y \in \mathcal{Y}} \mathbb{P}(y = y | \mathbf{x}) \right], \end{aligned} \quad (2)$$

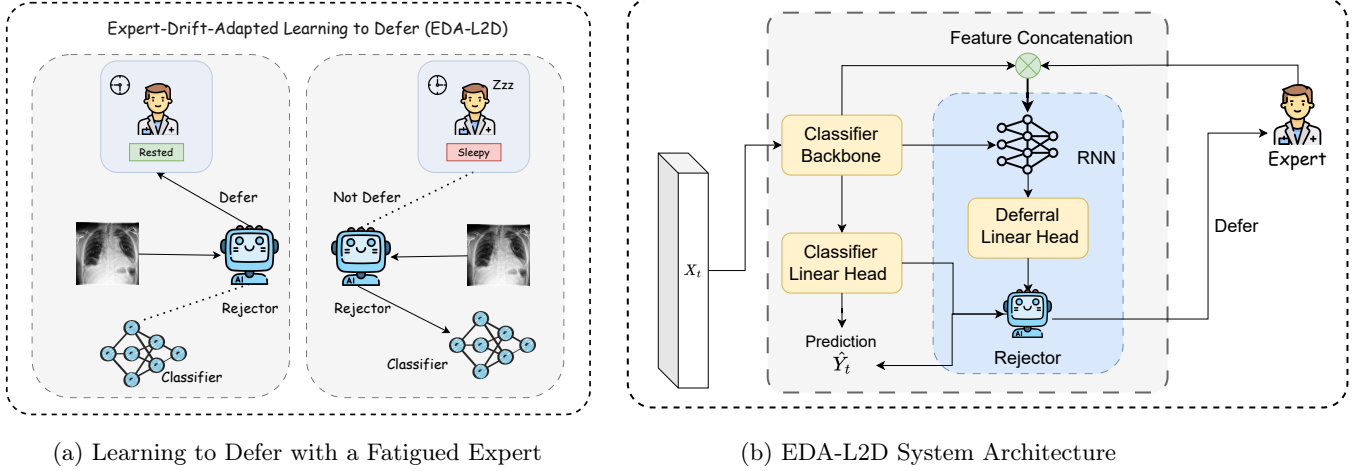
where  $\mathbb{P}(y | \mathbf{x})$  represents the label probability under the data generating process, and  $\mathbb{P}(m = y | \mathbf{x})$  is the probability of the expert making the correct prediction. The expert may have knowledge not available to the classifier, so they could outperform the Bayes optimal classifier.

### 2.3 Softmax Surrogate Loss

A consistent surrogate loss for the above  $L_{0-1}$  loss can be derived following the formulation from Mozannar and Sontag (2021). First, we consider an augmented label space that includes both the label space  $\mathcal{Y}$  and the rejection option  $\perp$ :  $\mathcal{Y}^\perp := \mathcal{Y} \cup \{\perp\}$ . Secondly, for a class  $k \in [1, K]$ , let  $g_k : \mathcal{X} \mapsto \mathbb{R}$ , and let  $g_\perp : \mathcal{X} \mapsto \mathbb{R}$  denote the rejection option. We can combine these  $K + 1$  with a loss resembling the cross-entropy loss for a softmax parameterization:

$$\begin{aligned} \phi_{\text{SM}}(g_1, \dots, g_K, g_\perp; \mathbf{x}, y, m) &= \\ &- \log \left( \frac{\exp\{g_y(\mathbf{x})\}}{\sum_{y' \in \mathcal{Y}^\perp} \exp\{g_{y'}(\mathbf{x})\}} \right) \\ &- \mathbb{I}[m = y] \log \left( \frac{\exp\{g_\perp(\mathbf{x})\}}{\sum_{y' \in \mathcal{Y}^\perp} \exp\{g_{y'}(\mathbf{x})\}} \right). \end{aligned} \quad (3)$$

Here, the first term maximizes  $g_k$  for the true label  $k$ . The second term maximizes the rejection function  $g_\perp$ , but only when the expert’s prediction is correct. At test time, the classifier takes the maximum over the classes:  $\hat{y} = h(\mathbf{x}) = \arg \max_{k \in [1, K]} g_k(\mathbf{x})$ . Similarly, we formulate the rejection function as  $r(\mathbf{x}) = \mathbb{I}[g_\perp(\mathbf{x}) \geq \max_k g_k(\mathbf{x})]$ . The minimizers  $g_1^*, \dots, g_K^*, g_\perp^*$  of  $\phi_{\text{SM}}$  also uniquely minimize the 0-1 loss from Equation 1,  $L_{0-1}(h, r)$ .



(a) Learning to Defer with a Fatigued Expert

(b) EDA-L2D System Architecture

Figure 2: (a) An example use case of our EDA-L2D framework in a setting with expert performance drift: a radiologist whose performance degrades over a workday. Our model monitors past outcomes to infer current expert reliability in real time, deferring to the expert when reliable and assigning cases to the model when the expert’s performance declines. (b) Overview of our expert drift adapted L2D framework. A streaming sequence of inputs is encoded by the backbone into features. At each timestep, the feature vector is concatenated with the expert’s previous prediction and passed to an RNN module. The classifier head outputs class logits and the defer head outputs a deferral score; a deferral gate then assigns the instance to either the expert or the classifier. Because the expert’s competence drifts over time, this design makes the L2D system time-aware and adaptive to temporal shifts.

### 3 EXPERT-DRIFT-ADAPTED LEARNING TO DEFER

This section introduces our *Expert-Drift-Adapted Learning to Defer* (EDA-L2D) framework, which extends L2D to account for non-stationarity in expert performance. Accordingly, we derive the corresponding softmax surrogate loss for this setting. We also propose multiple parameterizations, including one that uses a recurrent neural network to incorporate short-horizon temporal context into the deferral policy.

#### 3.1 Setting: Non-Stationary Expert

We consider the same setting as Section 2—L2D for multi-class classification—except now we assume the expert is non-stationary. Thus, instead of a fixed distribution  $\mathbb{P}(m \mid x)$ , the expert’s predictions are generated by  $\mathbb{P}_t(m_t \mid x)$ , with the subscript  $t \in \mathcal{T}$  denoting a time index. Note that we are *assuming the classification task itself is stationary*, i.e.  $y \sim \mathbb{P}(y \mid x)$ , which still has no time dependence.

To ground the notation in an example, consider an L2D system for radiology. The problem of forming a diagnosis or other prediction from the medical image itself is a static task, since we assume the distribution of patients and the mechanism that govern their health is not changing over time (or is at least changing so slowly as to be negligible, e.g. drift in hospital patient

demographics). Yet the radiologist who is paired with the L2D system will change, at the very least becoming more tired and distracted over the course of a 10+ hour shift. The expert drift may also be non-monotonic: perhaps her performance degrades over the course of a morning, but after lunch and a mid-day walk, the expert feels rejuvenated for a few more hours.

Returning to the technical details, our EDA-L2D system will have a classifier that is defined just as above:  $h : \mathcal{X} \rightarrow \mathcal{Y}$ . Again, the classifier is time-invariant since the prediction task itself is not time dependent. The difference, however, arises in the rejector:  $r : \mathcal{X} \times \mathcal{T} \mapsto \{0, 1\}$ , meaning the rejector is a function of both the feature space  $\mathcal{X}$  and time  $\mathcal{T}$ . While in the simplest case  $\mathcal{T}$  would be a scalar time index, we could also formulate  $\mathcal{T}$  as a feature space that describes the current state of the expert (e.g. tabular biomarkers).

#### 3.2 Learning Objective and Solutions

The learning objective is similar to that in Section 2 (equation 1), except now it takes the form of a summation over time:

$$\begin{aligned} L_{0-1}^{\mathcal{T}}(h, r) = \sum_{t \in \mathcal{T}} \mathbb{E}_{\mathbf{x}, y, m_t} & \left[ (1 - r(\mathbf{x}, t)) \mathbb{I}[h(\mathbf{x}) \neq y] \right. \\ & \left. + r(\mathbf{x}, t) \mathbb{I}[m_t \neq y] \right]. \end{aligned} \quad (4)$$

As the distribution of  $y$  does not depend on time, the classifier’s Bayes solution is just as before:  $h^*(\mathbf{x}) =$

$\arg \max_{y \in \mathcal{Y}} \mathbb{P}(y = y \mid \mathbf{x})$ . Yet the Bayes optimal rejector does change, becoming time-dependent like so:

$$r^*(\mathbf{x}, t) = \mathbb{I}\left[\mathbb{P}_t(m_t = y \mid \mathbf{x}) \geq \max_{y \in \mathcal{Y}} \mathbb{P}(y = y \mid \mathbf{x})\right].$$

This rejector simply rejects compares the expert's time-conditional

**Temporal Softmax Surrogate Loss** The softmax surrogate in equation 3 can be naturally extended to the temporal setting by introducing the time index  $t$ . Specifically, at each step we define

$$\begin{aligned} \phi_{\text{SM}}^t(g_1, \dots, g_K, g_{\perp}; \mathbf{x}, y, m_t) = & -\log \frac{\exp\{g_y(\mathbf{x})\}}{\sum_{y' \in \mathcal{Y}^{\perp}} \exp\{g_{y'}(\mathbf{x})\}} \\ & - \mathbb{I}[m_t = y] \log \frac{\exp\{g_{\perp}(\mathbf{x})\}}{\sum_{y' \in \mathcal{Y}^{\perp}} \exp\{g_{y'}(\mathbf{x})\}}. \end{aligned} \quad (5)$$

equation 5 is the same surrogate as equation 3 but evaluated *pointwise in time*: the class term promotes  $g_{y_t}(\mathbf{x}_t)$ , and the reject term promotes  $g_{\perp}(\mathbf{x}_t)$  only when the expert is correct at time  $t$ .

### 3.3 Expert Drift Aware Deferral Model

Formally, let  $\{(x_t, y_t, m_t)\}_{t=1}^T$  be a sequence with  $x_t \in \mathcal{X}$ ,  $y_t \in \mathcal{Y}$ , and expert output  $m_t \in \mathcal{Y}$ .

**Encoder.** Maps the raw input to a fixed-length representation used downstream.

$$f_t = \phi(x_t), \quad f_t \in \mathbb{R}^d. \quad (6a)$$

**Temporal state.** Aggregates short-horizon context by combining current features with the previous expert outcome; this is the sole place where temporal dependence enters.

$$z_t = \Psi(z_{t-1}, f_t, \hat{m}_{t-1}), \quad z_t \in \mathbb{R}^h. \quad (6b)$$

Here,  $\Psi$  is a lightweight sequence module. During training we use teacher forcing for  $\hat{m}_{t-1} \in \{0, 1\}$  (expert correct/incorrect at  $t-1$ ); at test time it is computed from realized routing and the expert's actual outcome.

**Heads.** Two linear heads read the shared state: one produces label logits, the other produces a deferral logit.

$$\begin{aligned} g_k(x_t) &= w_k^T z_t \quad (k \in [K]), \\ g_{\perp}(x_t) &= w_{\perp}^T z_t. \end{aligned} \quad (7)$$

Here,  $\{g_k(x_t)\}_{k=1}^K$  represents the model's confidence scores across all classes, with the predicted label chosen

by  $\arg \max_k g_k(x_t)$ . By contrast,  $g_{\perp}(x_t)$  quantifies the preference for deferral, indicating whether the system should rely on the expert instead of having the model predict one of the  $K$  classes.

**Rejector.** Defer when the deferral logit dominates the best class logit; otherwise predict.

$$h_t(x_t) = \arg \max_{k \in [K]} g_k(x_t), \quad (8)$$

$$r_t(x_t) = \mathbb{I}\left[g_{\perp}(x_t) \geq \max_{k \in [K]} g_k(x_t)\right]. \quad (9)$$

**System decision.** Combine the model and expert outputs according to the binary gate  $r_t(x_t)$ .

$$\hat{y}_t = (1 - r_t(x_t)) h_t(x_t) + r_t(x_t) m_t. \quad (10)$$

The intuition behind this formulation is that the classifier and rejector should not operate solely on the current input but instead incorporate temporal context that reflects the expert's evolving reliability. By conditioning the recurrent state  $z_t$  on both the encoded input  $f_t$  and the previous correctness indicator  $\hat{m}_{t-1}$ , the system adaptively tracks fluctuations in expert performance. The classifier head then focuses on predicting the label from this time-dependent state, while the deferral head directly estimates whether the expert should be trusted at the current step.

### 3.4 Baselines

To make comparisons precise, all methods are cast within the L2D paradigm. All methods trained with the same  $L_{\text{CE}}$  objective; methods differ only in how the deferral policy is parameterized across time.

- **Native L2D(baseline):** a time-invariant L2D policy with a single head shared across all steps, yielding one routing rule for the entire sequence.
- **EDA-L2D, Per-step param.:** a collection of independent L2D policies, one head per step, capturing step-specific effects without any temporal coupling.
- **EDA-L2D, RNN param.:** a sequence-aware L2D policy whose routing depends on the evolving context across time via summaries of past behavior in addition to current inputs.

## 4 EXPERIMENTS

We evaluate our proposed EDA-L2D framework through a progression from controlled simulations

to heterogeneous real-world tasks with real human-annotated data. We train EDA-L2D and baseline models on three benchmarks spanning distinct modalities and annotation regimes: **CIFAR-10** (image classification), **CheXpert** (chest X-ray classification) and **HateSpeech** (text moderation).

#### 4.1 CIFAR10

**Task and Data.** We study standard image classification on CIFAR-10 (Krizhevsky, 2009). The dataset contains 60,000 color images at  $32 \times 32$  resolution from ten object categories (airplane, automobile, bird, cat, deer, dog, frog, horse, ship, truck), with 50,000 training images and 10,000 test images. Given an input image  $x$ , the goal is to output either a predicted class label or defer the decision to the expert. For our experiments, we first arrange the 50,000 training images into sequences and perform a 90/10 split into training and validation sets at the sequence level, ensuring that each sequence appears in exactly one set. The official 10,000-image test set is used for final evaluation.

**Synthetic Expert** In this experiment, we constructed a simple synthetic expert to provide a controlled baseline. Following the setup of Mozannar and Sontag (2021), we assume that the expert initially has full knowledge of all classes, i.e.,  $K=10$ . The expert’s accuracy is then designed to decrease linearly over time from 100% accuracy at the beginning to 50% accuracy at  $T=50$ . At each timestep, the expert’s prediction is sampled according to a Bernoulli trial with the corresponding time-dependent accuracy, thereby generating stochastic outputs that reflect the intended accuracy trajectory.

**Classifier and EDA-L2D architecture.** For the classifier, we adopt WRN-28-4 with standard CIFAR-10 normalization. For deferral, we take the features output by the classifier, concatenate them with a one-step indicator of whether the expert was correct at  $t-1$  and a normalized timestep indicator, and pass this concatenated vector through a 1-layer GRU with 256 hidden units. The GRU output is then fed to a fully connected deferral head that produces a single defer logit.

**Training.** Training proceeds in two stages. First, the backbone are optimized with cross-entropy, using SGD (momentum 0.9, weight decay  $5 \times 10^{-4}$ ), cosine-annealed learning rate, batch size 128, and no dropout. The model minimizes cross-entropy for 200 epochs; this yields 90.27% test accuracy on CIFAR-10. We then fine-tune the entire network end-to-end using the L2D softmax surrogate loss: the classifier backbone continues training with SGD using cosine annealing over

25000 total iterations, while GRU and the two classifier heads use Adam driven by a custom cosine-then-hold schedule implemented via LambdaLR (cosine anneal for the first 25 epochs, then hold for the remaining 25 of a 50-epoch run).

**Results.** In this experiment we considered a simple expert model with linearly decaying accuracy from 100% to 50%. Since the classifier achieves an accuracy of 90.47%, we would expect fewer samples to be deferred to the expert once the expert’s performance falls below the classifier’s. Our results confirm this intuition: as shown in Figure 3b, at time  $t=10$  our RNN-based EDA-L2D and the per-step EDA-L2D adapt their deferral rate accordingly. Moreover, Figure 3a demonstrates that EDA-L2D achieves higher overall system accuracy in both settings. These findings indicate that our method makes more appropriate allocations both before and after the crossing point, correctly assigning more samples to the expert when its accuracy is higher and shifting them to the classifier once the expert’s performance declines.

#### 4.2 CheXpert

**Task.** We study chest X-ray classification on CheXpert(Irvin et al., 2019) with the standard 14 observations, framing the problem as *per-task, per-timestep* binary decisions over image sequences of length  $T$ . At each timestep  $t \in \{1, \dots, T\}$  and for each task  $k \in \{1, \dots, 14\}$ , the system must either output a class prediction or defer to an external expert.

**Expert.** Following Mozannar and Sontag (2021), we simulate a class-dependent, time-varying expert with two accuracy levels,  $p$  and  $q$ . A designated confounding class receives a lower base accuracy, while all other classes receive a higher one. Over time, both accuracies decay linearly at fixed rates, with a small positive floor to avoid vanishing performance. In our experiments, we set the base accuracies to  $p=1.0$  (non-confounding) and  $q=0.7$  (confounding), apply decay rates of  $d=0.05$  and  $\delta=0.035$ , and  $T=10$ . The expert label is generated as  $\text{Bernoulli}(q_t)$  if the example is confounding and  $\text{Bernoulli}(p_t)$  otherwise.

**Data.** We use the downsampled CheXpert release and keep 14 one-vs-rest targets and a binary mask that suppresses tasks marked uncertain or missing under CheXpert’s label encoding. All images are converted to three channels, normalized, and resized to ImageNet-compatible resolution; training augmentation uses random resized crops, horizontal flips, and random rotations up to  $15^\circ$ . Dataset splits are patient-disjoint with an 80/10/10 train/validation/test partition.

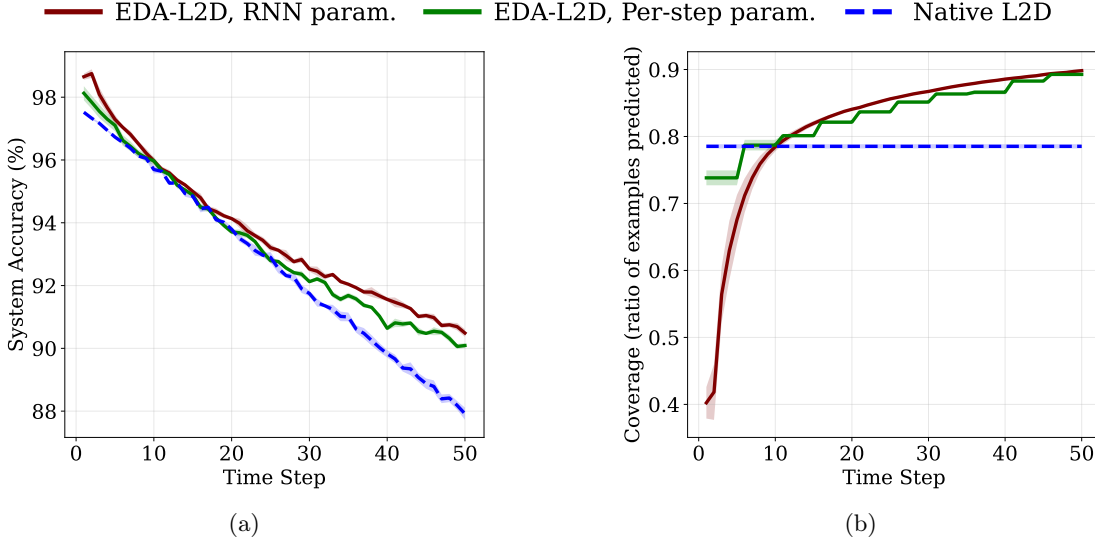


Figure 3: Plot of system accuracy (a) and coverage(proportion of classifier taken examples) (b) comparing our methods with the baseline on the CIFAR-10 test set across 50 time steps. We evaluate using a toy expert whose accuracy linearly decays from 100% to 50%. Error bars represent standard deviations over 10 runs.

**Classifier and EDA-L2D architecture.** Following Irvin et al. (2019), we use a DenseNet-121 backbone initialized with ImageNet pretraining. We add two heads to the classifier backbone. The first is a per-class classifier that takes the CNN feature at time step  $t$  and outputs two logits (negative vs. positive). The second is a one-layer LSTM with 1024 hidden units that takes the CNN feature together with the expert’s previous predictions and produces one deferral logit per class. At inference, for each class, we form a three-way distribution—negative (no disease), positive (diseased), and defer—and we defer to the expert whenever the defer score exceeds the larger of the two class scores; otherwise, we use the classifier’s prediction.

**Training.** We train the model in two stages over a total of four epochs. In the first stage, we pre-train the CNN and classification head with standard cross-entropy for three epochs, averaging the loss over samples. In the second stage, we fine-tune the entire network end-to-end for one epoch with  $L_{CE}$ , accumulating losses across each sequence and normalizing by its length  $T$ . All four epochs use Adam (learning rate  $1 \times 10^{-4}$ , weight decay  $1 \times 10^{-5}$ ) with a Reduce-on-Plateau scheduler.

**Results** In Fig. 4, we compare our method with the baseline L2D approach and the per-step EDA-L2D on the CheXpert dataset with our synthetic expert. On the Lung Opacity and Ateletasis tasks, our approach clearly outperforms native L2D and performs on par with the per-step EDA-L2D; on the Consolidation task, RNN-based EDA-L2D outperforms both the per-step

EDA-L2D and native L2D.

### 4.3 Hatespeech

We study detection of abusive content on Twitter posts using the Davidson et al. (2017) corpus of 24,783 English tweets annotated into three mutually exclusive classes: *hate speech*, *offensive but not hate*, and *neither*.

**Expert.** We follow prior work that uses the Twitter-AAE lexical model to probabilistically identify tweets written in African-American English (AAE) and binarize group membership with a 0.5 threshold(Blodgett et al., 2016). We instantiate a synthetic fair expert whose accuracy is identical across demographics. At timestep  $t$ , the expert’s correctness probability decays linearly from 1.0 to 0.5 over the sequence. For each tweet, we sample a Bernoulli variable to decide whether the expert outputs the ground-truth label; if not, the expert predicts uniformly at random among the remaining classes. We construct sequences of length  $T=10$  for evaluation.

**Classifier architecture.** Our hate-speech classifier models are lightweight TextCNNs. Tweets are tokenized with spaCy and mapped to a 25k vocabulary; embeddings are initialized with GloVe-6B (100d) and fine-tuned. The encoder applies three parallel convolutional filters of widths 3, 4, and 5 (300 channels each) over the embedding matrix, followed by ReLU and max-over-time pooling. The pooled features are concatenated, passed through dropout (0.5), and fed to a linear classifier.

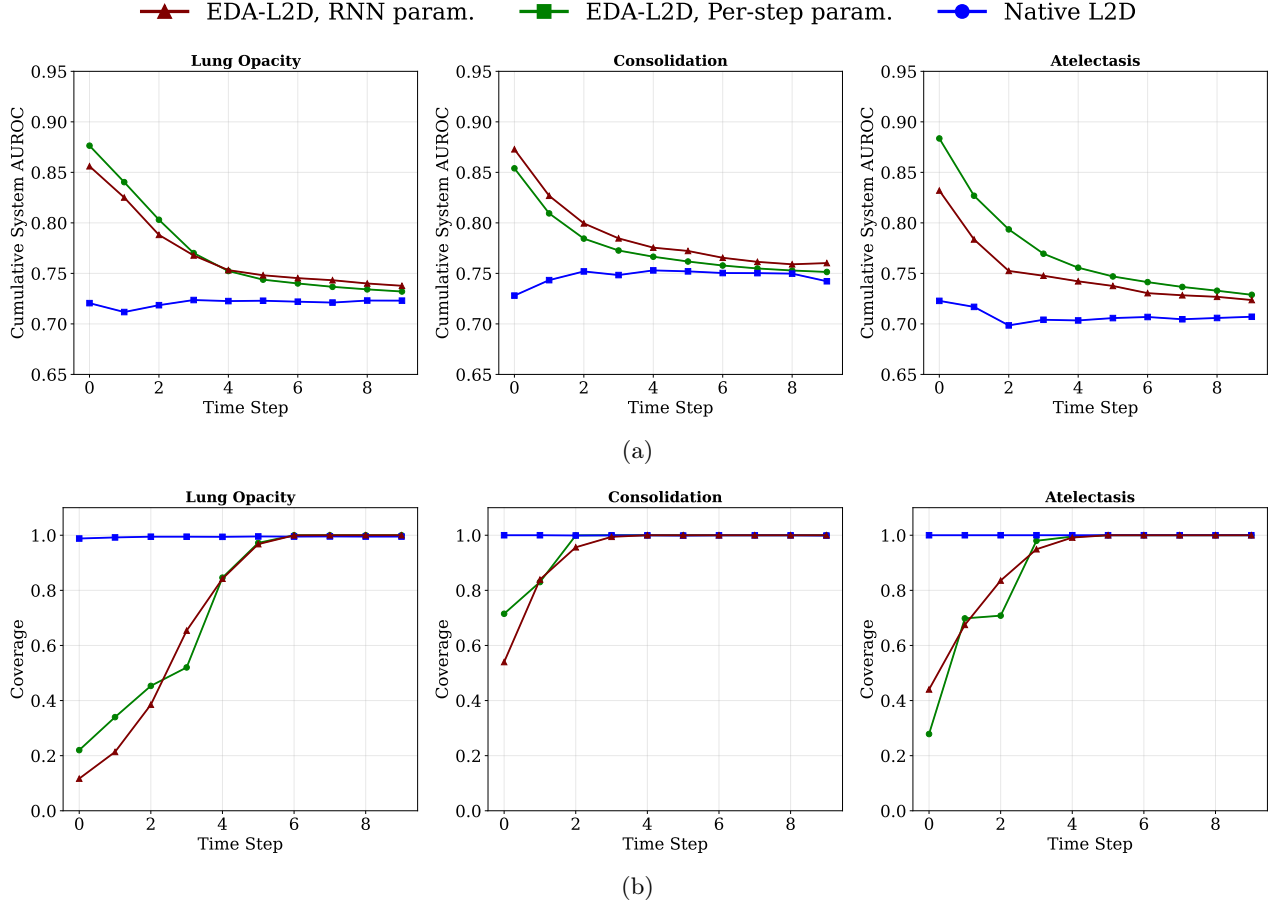


Figure 4: Plot of system accuracy (a) and coverage(ratio of classifier-taken examples) (b) comparing our methods with the baseline on the CheXpert dataset. For each timestep  $t$ , we evaluate on sequences built from a 10% patient-ID subset, using a fair expert whose accuracy decays linearly from 100% to 50%.

**EDA-L2D architecture.** We employ a TextCNN encoder to obtain a per-timestep feature representation for each tweet in a length- $T$  sequence. To model temporal dependencies and expert reliability, we concatenate a binary indicator of the expert’s correctness at the previous timestep to the CNN feature and feed the resulting vector into a single-layer LSTM with 256 hidden units. The TextCNN encoder feeds a fully connected classification head that outputs three logits (hate, offensive, neither), while the LSTM feeds a fully connected deferral head that outputs a single defer logit. Concatenating these yields a four-way prediction over hate, offensive, neither, defer. At inference, we defer to the expert when the defer logit exceeds the maximum of the three class logits; otherwise, the classifier’s prediction is returned.

**Results.** From Fig. 5a, we observe that our model trained on the HateSpeech dataset demonstrates a clear advantage. In terms of system accuracy, our method consistently outperforms both the native L2D and per-

step EDA-l2D approach, with an average margin of 1.26% and 0.70%, respectively. Moreover, from Fig. 5b, we observe that our method identifies more favorable timesteps than the per-step model at which the system coverage surpasses that of the general baseline, resulting in higher system accuracy at those points.

## 5 RELATED WORK

**Learning to Defer (L2D).** Early work on classifiers that can choose to reject or abstain instead of making a prediction (Chow, 1957) inspired more recent work on the modern formulation of the Learning to Defer (L2D) framework (Madras et al., 2018). This work has been expanded in recent years to address several limitations, including mis-calibration (Verma and Nalisnick, 2022; Cao et al., 2023), underfitting (Narasimhan et al., 2022), realizable consistency (Mozannar et al., 2023), sample complexity (Charusai et al., 2022), data scarcity (Hemmer et al., 2023), and deferral to multiple experts (Tailor et al., 2024). However, these approaches

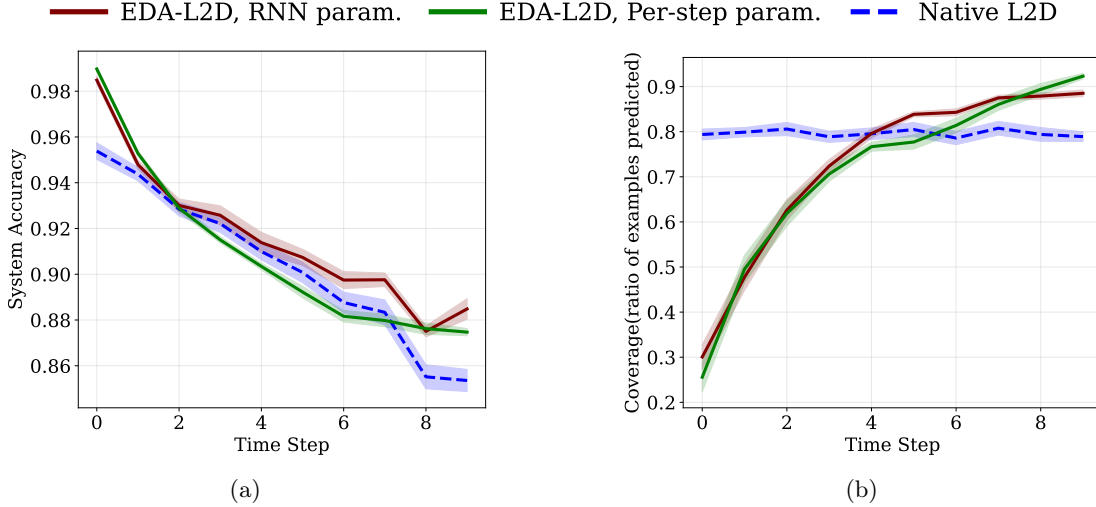


Figure 5: Plot of system accuracy (a) and coverage(ratio of classifier–taken examples) (b) comparing our methods with the baseline on the HateSpeech dataset across 10 time steps. We simulate using a toy expert whose accuracy decays linearly from 100% to 50% over 10 timesteps. Results are averaged over 10 runs, with error bars showing standard deviations.

employ a more capable model or simple simulation as the expert for deferral, failing to consider how deferral to a *human expert* may differ from a synthetic expert.

**Temporal shifts in human performance.** In many high-stakes domains, human performance shift over time (due to fatigue or other cognitive factors) are well-documented and widely studied. Fatigue is extremely common in high-stakes domains and long-horizon tasks, such as radiology (Bruni et al., 2012), automated driving (Figalová et al., 2024), air traffic control (Peukert et al., 2023), and flying planes (Pan et al., 2022). Beyond affecting surface-level performance on these tasks, fatigue physically affects the brain, causing reduced alertness and vigilance that can be measured directly, e.g. using EEG signals (Peukert et al., 2023). Besides fatigue, human decision-making is heavily influenced by cognitive biases, many of which adapt a human’s reliability over time – such as the availability heuristic (Tversky and Kahneman, 1973), gambler’s fallacy (Kovic and Kristiansen, 2019), delay discounting (Kurth-Nelson et al., 2012), and the recency bias (Turvey and Freeman, 2012). Our method explicitly accounts for and models these variations in human performance, enabling improved system performance on true human-AI collaboration tasks.

**L2D under non-stationarity.** Recent work on L2D has begun to account for this kind of expert variability. For instance, *Sequential Learning-to-Defer* (SLTD) (Joshi et al., 2023) models these temporal dynamics by framing deferral in sequential decision-making settings, using a model-based reinforcement learning approach

to account for variance in expert decision-making. However, while SLTD advances beyond static L2D by framing deferral as a sequential decision-making problem and allowing for limited expert–policy deviations, it is not explicitly designed to handle substantial and systematic expert drift. Our approach addresses this by computing predictions of expert accuracy on each example and explicitly accounting for the history of previous examples, building knowledge of temporal variation in performance explicitly into our model.

## 6 CONCLUSION & FUTURE WORK

We propose *expert drift adapted Learning to Defer* (*EDA-L2D*), a framework that enables improved generalization to real human experts not seen during training by explicitly modeling temporal variance in human expert performance – variance that is common and caused by a wide variety of factors, such as fatigue and cognitive biases. We achieve this by explicitly incorporating time and prediction history into the L2D model, allowing the model to learn representations of the expert that vary with each time-step and dynamically adapt to the expert’s behavior to achieve improved deferral decisions and greater human-AI team performance.

Future work may consider how to model other human-specific performance variation within the L2D model, as well as how to create a human-aware deferral model that can be effectively applied even in very data-scarce regimes.

## References

- Zeynep Akata, Dan Balliet, Maarten de Rijke, Frank Dignum, Virginia Dignum, A. E. Eiben, Antske Fokkens, Davide Grossi, Koen V. Hindriks, Holger Hoos, Haley Hung, Catholijn Jonker, Christof Monz, Mark Neerincx, Frans Oliehoek, Henry Prakken, Stefan Schlobach, Linda C. van der Gaag, Frank van Harmelen, Herke van Hoof, M. Birna van Riemsdijk, Aimee van Wynsberghe, Rineke Verbrugge, Bart Verheij, Paul Vossen, and Max Welling. A research agenda for hybrid intelligence: Augmenting human intellect with collaborative, adaptive, responsible, and explainable artificial intelligence. *Computer*, 53(8):18–28, 2020. doi: 10.1109/MC.2020.2996587. URL <https://www.computer.org/csdl/magazine/co/2020/08/09153877/11UB5gL2CnS>.
- Su Lin Blodgett, Lisa Green, and Brendan O’Connor. Demographic dialectal variation in social media: A case study of african-american english, 2016. URL <https://arxiv.org/abs/1608.08868>.
- Silvio G Bruni, Eric Bartlett, and Eugene Yu. Factors involved in discrepant preliminary radiology resident interpretations of neuroradiological imaging studies: a retrospective analysis. *American Journal of Roentgenology*, 198(6):1367–1374, 2012.
- Yuzhou Cao, Hussein Mozannar, Lei Feng, Hongxin Wei, and Bo An. In defense of softmax parametrization for calibrated and consistent learning to defer, 2023. URL <https://arxiv.org/abs/2311.01106>.
- Mohammad-Amin Charusaie, Hussein Mozannar, David Sontag, and Samira Samadi. Sample efficient learning of predictors that complement humans, 2022. URL <https://arxiv.org/abs/2207.09584>.
- C. K. Chow. An optimum character recognition system using decision functions. *IRE Transactions on Electronic Computers*, EC-6(4):247–254, 1957. doi: 10.1109/TEC.1957.5222035.
- Thomas Davidson, Dana Warmsley, Michael Macy, and Ingmar Weber. Automated hate speech detection and the problem of offensive language, 2017. URL <https://arxiv.org/abs/1703.04009>.
- Dominik Dellermann, Philipp Ebel, Matthias Söllner, and Jan Marco Leimeister. Hybrid intelligence. *Business & Information Systems Engineering*, 61(5):637–643, 2019. doi: 10.1007/s12599-019-00595-2. URL <https://link.springer.com/article/10.1007/s12599-019-00595-2>.
- Nikol Figalová, Hans Joachim Bieg, Michael Schulz, Jürgen Pichen, Martin Baumann, Lewis Chuang, and Olga Pollatos. Fatigue and mental underload further pronounced in l3 conditionally automated driving: Results from an eeg experiment on a test track. *ArXiv preprint arXiv:2405.18114*, 2024. L3 supervisor sleepiness increases with prolonged monitoring; EEG measures show drift in alertness.
- Patrick Hemmer, Lukas Thede, Michael Vössing, Johannes Jakubik, and Niklas Kühl. Learning to defer with limited expert predictions, 2023. URL <https://arxiv.org/abs/2304.07306>.
- Jeremy Irvin, Pranav Rajpurkar, Michael Ko, Yifan Yu, Silviana Ciurea-Ilcus, Chris Chute, Henrik Marklund, Behzad Haghgoo, Robyn Ball, Katie Shpanskaya, Jayne Seekins, David A. Mong, Safwan S. Halabi, Jesse K. Sandberg, Ricky Jones, David B. Larson, Curtis P. Langlotz, Bhavik N. Patel, Matthew P. Lungren, and Andrew Y. Ng. Chexpert: A large chest radiograph dataset with uncertainty labels and expert comparison, 2019. URL <https://arxiv.org/abs/1901.07031>.
- Shalmali Joshi, Sonali Parbhoo, and Finale Doshi-Velez. Learning-to-defer for sequential medical decision-making under uncertainty. *Transactions on Machine Learning Research*, 2023. URL <https://arxiv.org/abs/2109.06312>.
- C. Peterson Joshua M. Battleday Ruairidh L. Griffiths Thomas and Olga Russakovsky. Human uncertainty makes classification more robust. In *Proceedings of the IEEE/CVF International Conference on Computer Vision (ICCV)*, pages 9617–9626, 2019. doi: 10.1109/ICCV.2019.00971. URL <https://arxiv.org/abs/1908.07086>.
- Ece Kamar. Directions in hybrid intelligence: Complementing ai systems with human intelligence. In *Proceedings of the Twenty-Fifth International Joint Conference on Artificial Intelligence (IJCAI-16)*, 2016. URL <https://www.microsoft.com/en-us/research/wp-content/uploads/2016/02/HybridIntelligence.pdf>. Position paper outlining research directions for human-AI systems.
- Marko Kovic and Silje Kristiansen. The gambler’s fallacy fallacy (fallacy). *Journal of Risk Research*, 22(3):291–302, 2019. doi: 10.1080/13669877.2017.1378248. URL <https://doi.org/10.1080/13669877.2017.1378248>.
- Alex Krizhevsky. Learning multiple layers of features from tiny images. Technical report, University of Toronto, 2009. URL <https://www.cs.toronto.edu/~kriz/learning-features-2009-TR.pdf>. Technical Report.
- Zeb Kurth-Nelson, Warren Bickel, and A. David Redish. A theoretical account of cognitive effects in delay discounting. *European Journal of Neuroscience*, 35(7):1052–1064, 2012. doi: <https://doi.org/10.1111/j.1460-9568.2012.08058.x>. URL <https://onlinelibrary.wiley.com/doi/abs/10.1111/j.1460-9568.2012.08058.x>.

- Eric Legler, Darío Cuevas Rivera, Sarah Schwöbel, Ben J. Wagner, and Stefan Kiebel. Cognitive computational model reveals repetition bias in a sequential decision-making task. *Communications Psychology*, 3(1):92, 2023. doi: 10.1038/s44271-025-00271-0.
- David Madras, Toniann Pitassi, and Richard Zemel. Predict responsibly: Improving fairness and accuracy by learning to defer, 2018. URL <https://arxiv.org/abs/1711.06664>.
- Hussein Mozannar and David Sontag. Consistent estimators for learning to defer to an expert, 2021. URL <https://arxiv.org/abs/2006.01862>.
- Hussein Mozannar, Hunter Lang, Dennis Wei, Prasanna Sattigeri, Subhro Das, and David Sontag. Who should predict? exact algorithms for learning to defer to humans, 2023. URL <https://arxiv.org/abs/2301.06197>.
- Harikrishna Narasimhan, Wittawat Jitkrittum, Aditya K Menon, Ankit Rawat, and Sanjiv Kumar. Post-hoc estimators for learning to defer to an expert. In S. Koyejo, S. Mohamed, A. Agarwal, D. Belgrave, K. Cho, and A. Oh, editors, *Advances in Neural Information Processing Systems*, volume 35, pages 29292–29304. Curran Associates, Inc., 2022. URL [https://proceedings.neurips.cc/paper\\_files/paper/2022/file/bc8f76d9caadd48f77025b1c889d2e2d-Paper-Conference.pdf](https://proceedings.neurips.cc/paper_files/paper/2022/file/bc8f76d9caadd48f77025b1c889d2e2d-Paper-Conference.pdf).
- T. Pan et al. Research on the identification of pilots' fatigue status based on fnirs signals and deep models. *Aerospace*, 9(3):173, 2022. doi: 10.3390/aerospace9030173. Identifies pilot fatigue using brain signals; performance drift with fatigue.
- M. Peukert et al. Subjective and objective fatigue dynamics in air traffic control. *Journal of Sleep Research*, 2023. Showing increase in subjective fatigue and drop in vigilance toward end of evening shifts for air traffic controllers.
- Dharmesh Tailor, Aditya Patra, Rajeev Verma, Putra Manggala, and Eric Nalisnick. Learning to defer to a population: A meta-learning approach, 2024. URL <https://arxiv.org/abs/2403.02683>.
- B.E. Turvey and J.L. Freeman. Jury psychology. In V.S. Ramachandran, editor, *Encyclopedia of Human Behavior (Second Edition)*, pages 495–502. Academic Press, San Diego, second edition edition, 2012. ISBN 978-0-08-096180-4. doi: <https://doi.org/10.1016/B978-0-12-375000-6.00216-0>. URL <https://www.sciencedirect.com/science/article/pii/B9780123750006002160>.
- Amos Tversky and Daniel Kahneman. Availability: A heuristic for judging frequency and probability. *Cognitive Psychology*, 5(2):207–232, 1973. ISSN 0010-0285. doi: [https://doi.org/10.1016/0010-0285\(73\)90033-9](https://doi.org/10.1016/0010-0285(73)90033-9). URL <https://www.sciencedirect.com/science/article/pii/0010028573900339>.
- Anne E. Urai, Jan Willem de Gee, Konstantinos Tsetsos, and Tobias H. Donner. Choice history biases subsequent evidence accumulation. *eLife*, 8:e46331, 2019. doi: 10.7554/eLife.46331.
- Didrika S. van de Wouw, Ryan T. McKay, and Nicholas Furl. Biased expectations about future choice options predict sequential economic decisions. *Communications Psychology*, 2(1):119, 2024. doi: 10.1038/s44271-024-00172-8.
- Rajeev Verma and Eric Nalisnick. Calibrated learning to defer with one-vs-all classifiers, 2022. URL <https://arxiv.org/abs/2202.03673>.

## Checklist

1. For all models and algorithms presented, check if you include:
  - (a) A clear description of the mathematical setting, assumptions, algorithm, and/or model. [Yes]
  - (b) An analysis of the properties and complexity (time, space, sample size) of any algorithm. [Yes]
  - (c) (Optional) Anonymized source code, with specification of all dependencies, including external libraries. [Yes]
2. For any theoretical claim, check if you include:
  - (a) Statements of the full set of assumptions of all theoretical results. [Not Applicable]
  - (b) Complete proofs of all theoretical results. [Not Applicable]
  - (c) Clear explanations of any assumptions. [Not Applicable]
3. For all figures and tables that present empirical results, check if you include:
  - (a) The code, data, and instructions needed to reproduce the main experimental results (either in the supplemental material or as a URL). [Yes]
  - (b) All the training details (e.g., data splits, hyperparameters, how they were chosen). [Yes]
  - (c) A clear definition of the specific measure or statistics and error bars (e.g., with respect to the random seed after running experiments multiple times). [Yes]
  - (d) A description of the computing infrastructure used. (e.g., type of GPUs, internal cluster, or cloud provider). [Yes]

4. If you are using existing assets (e.g., code, data, models) or curating/releasing new assets, check if you include:

- (a) Citations of the creator If your work uses existing assets. [Yes]
- (b) The license information of the assets, if applicable. [Not Applicable]
- (c) New assets either in the supplemental material or as a URL, if applicable. [Yes]
- (d) Information about consent from data providers/curators. [Not Applicable]
- (e) Discussion of sensible content if applicable, e.g., personally identifiable information or offensive content. [Not Applicable]

5. If you used crowdsourcing or conducted research with human subjects, check if you include:

- (a) The full text of instructions given to participants and screenshots. [Not Applicable]
- (b) Descriptions of potential participant risks, with links to Institutional Review Board (IRB) approvals if applicable. [Not Applicable]
- (c) The estimated hourly wage paid to participants and the total amount spent on participant compensation. [Not Applicable]